TECHNICAL RESEARCH REPORT

SYSTEMS RESEARCH CENTER

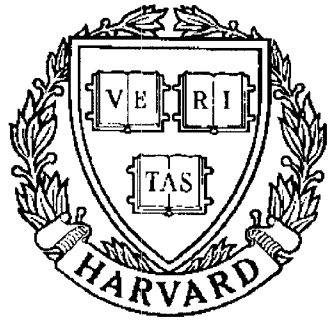

Supported by the National Science Foundation Engineering Research Center Program (NSFD CD 8803012), the University of Maryland, Harvard University, and Industry

Nonlinear Dynamics of Axial Flow Compressors: A Parametric Study

by D -C. Liaw , R.A. Adomaitis and E.H. Abed

TR 91-32

NONLINEAR DYNAMICS OF AXIAL FLOW COMPRESSORS: A PARAMETRIC STUDY

Der-Cherng Liaw,*† Raymond A. Adomaitis* and Eyad H. Abed*†

*Systems Research Center
†Department of Electrical Engineering
University of Maryland
College Park, MD 20742 USA

Abstract

This paper presents the analysis of the dynamics of a representative axial flow compressor model, emphasizing the influence of two important control parameters. These are a nondimensional parameter B (previously introduced by Greitzer (1976) as a primary determinant of post-stall behavior) and the setting of the throttle line. Greitzer's lumped-parameter model is employed in this study, with a specific choice of compressor and throttle characteristics. Our analysis shows the presence of a rich variety of global as well as local bifurcations as the two control parameters are varied. The analysis leads to a characterization of compressor operation into three major zones: the stalled zone, the pre-stall zone, and the normal (unstalled) zone. Simulation results demonstrate the qualitatively different dynamical behaviors within each regime of parameter space.

Manuscript: March 1991

1. Introduction

Recently, the dynamics of axial flow compressors has attracted considerable attention [1]-[7]. Among these studies, Greitzer [1] introduced a nondimensional parameter B and show-ed that, for a compressor operating near its maximum achievable pressure rise and subjected to a moderate disturbance, one may observe either a large amplitude oscillation (known as "surge"), or a very inefficient operation at constant mass flow and pressure rise (known as "rotating stall"). In addition, such behaviors were found to be strongly dependent upon the value of B. Based on Greitzer's model, a global bifurcation of an unstable periodic solution (antisurge oscillation) and a stable periodic solution (surge limit cycle) were found and used to study these stall behaviors from the viewpoint of bifurcation theory [3]. The presence of the global bifurcation of the surge and antisurge periodic solutions noted in [3] depends strongly on the assumed compressor characteristic. Indeed, the cubic characteristic used in [6] only supports the existence of a stable periodic oscillation, but does not support the existence of an unstable periodic solution, while the more complicated algebraic model of the characteristic of [3] does support the presence of both oscillations.

This paper continues the study of axial flow compressor dynamics begun in [3], emphasizing the combined effect of two control parameters: the setting of throttle line and the value of the B-parameter. As mentioned above, the dynamic behavior of the axial flow compressor depend on the model of the compressor characteristic. In this paper, the algebraic model of the compressor characteristic introduced in [3] is employed. Using the lumped parameter model proposed by Greitzer [1], we observe a rich variety of global and local bifurcations as two parameters are varied. Our analysis reveals three major regimes of compressor operation: the stalled zone, the pre-stall zone, and the normal (unstalled) zone. The numerical continuation and bifurcation analysis package AUTO [8] and extensive simulations are employed to evaluate the system's behavior. The numerical techniques consist of continuation of fixed points and limit cycles with respect to B, and continuation of bifurcation-point branches of fixed points and limit cycles in the two-parameter plane. Phase portraits are constructed by simulation to illustrate the distinctly-different dynamical behaviors associated with each regime of parameter space.

In [3], the dynamics for the stalled zone were studied for a fixed setting of the throttle line. The present results corroborate those in [3]. In particular, in the stalled zone and for small values of B, the rotating stall point is found to be globally asymptotically stable. However, as the value of B is increased, two large amplitude periodic solutions appear around the rotating stall point. These solutions consist of a stable periodic solution (limit cycle) encircling an unstable periodic solution. In this case, the rotating stall point is locally stable. As B increases further, the unstable periodic solution is observed to shrink and finally collapse onto the rotating stall point (which is rendered unstable in a subcritical Hopf bifurcation), while the stable periodic solution grows in amplitude resulting in a stable oscillation, the so-called "deep surge." Simulation results are given in Section 3, demonstrating these observations for both the second-order simplified model of [3] and the full fourth-order model of [1].

It has been shown [3] that the bifurcation behavior of the full fourth-order model of the compressor can be captured by a second-order simplified model. In the present study of the time responses of the compressor within the two remaining parameter zones (pre-stall and normal), we consider only the second-order simplified model of [3]. In general, as discussed in Section 4, there are two types of behavior of the compressor within the normal unstalled zone. The first occurs for small γ and is characterized by the presence of two periodic oscillations for the compressor dynamics: a stable limit cycle encircling an unstable periodic orbit and a locally stable fixed point. These oscillations are born and disappear at two different cyclic fold bifurcations as B varies. (A *cyclic fold* bifurcation is a common term for a saddle-node bifurcation of periodic orbits.) The other behavior occurs for large γ, for which the unstalled equilibrium point of the system is globally asymptotically stable, regardless of the value of B. In the pre-stall zone, the dynamical behavior of the compressor is found to be more complicated and to strongly depend on the throttle line position and the value of B. Details are given in Section 5.

2. Greitzer's Lumped-Parameter Model

A fourth-order lumped parameter model for the dynamics of an axial flow compressor has been introduced by Greitzer [1]. This model consists of the following set of ordinary

differential equations (using the notation of [3]):

$$\frac{d\dot{m}_C}{dt} = B(C - \Delta P), \tag{1}$$

$$\frac{d\dot{m}_T}{dt} = (\frac{B}{G})(\Delta P - F), \tag{2}$$

$$\frac{d\Delta P}{dt} = (\frac{1}{B})(\dot{m}_C - \dot{m}_T), \tag{3}$$

$$\frac{dC}{dt} = (\frac{1}{\tau})(C_{ss} - C), \tag{4}$$

where

$$F = (\frac{A_C^2}{A_T^2})\dot{m}_T^2. \tag{5}$$

Here, $\dot{m}_C$ (resp. $\dot{m}_T$) denotes the nondimensional compressor (resp. throttle) mass flow, ΔP (resp. C) denotes the nondimensional plenum (resp. compressor) pressure rise, and C_{ss} and F denote the nondimensional steady state compressor pressure rise and the nondimensional throttle pressure drop, respectively. The definition of the three parameters, B, G, and τ, in Eqs. (1)-(4) in terms of physical system parameters is given in [1]. τ denotes the relaxation time constant and B is proportional to rotor speed. In this paper, we set $G = 0.36$, as in [1]. In Eq. (5), A_T and A_C denote the cross-sectional areas of the throttle and compressor, respectively. The steady state compressor characteristic C_{ss} (for an axial flow compressor) is often modeled as a function of $\dot{m}_C$. An example of such a characteristic is depicted in Figure 1.

It is observed from Eqs. (1)-(4) that, at an equilibrium point,

$$C = C_{ss} = \Delta P = F \tag{6}$$

and

$$\dot{m}_C = \dot{m}_T. \tag{7}$$

Therefore, an equilibrium point of (1)-(4) occurs at the intersection of the compressor and throttle characteristics, graphed relative to the independent variable $\dot{m}_C$ (or, equivalently, $\dot{m}_T$).

The relaxation time constant τ is usually small. It has been shown [3] that, for small τ, the time response of the full fourth-order model is approximated by that of the reduced second-order model

$$\frac{d\dot{m}_C}{dt} = B(C_{ss} - \Delta P), \tag{8}$$

$$\frac{d\Delta P}{dt} = (\frac{1}{B})(\dot{m}_C - \gamma\sqrt{\Delta P}) \tag{9}$$

with

$$\gamma := \frac{A_T}{A_C}. \tag{10}$$

It is observed from Eq. (10) that closing the throttle corresponds to reducing the value of γ. This can be seen in Figure 1, where the throttle line shifts to the left as γ is reduced. In this paper, we study the time response of the axial flow compressor dynamics (1)-(4) as a function of γ and B using extensive computer simulations and numerical continuation of equilibrium solutions. The compressor characteristic assumed here is shown in Figure 1; the mathematical formula used to generate this characteristic is not given here for brevity.

3. Stalled Zone Dynamics

In this section, we study the time response of the compressor dynamics (1)-(4) for $\gamma < 0.41$ (i.e., Zone I behavior). A typical time response for the simplified model (8), (9) with respect to B can be seen in the bifurcation diagram of Figure 2.

To understand the bifurcation behavior illustrated in Figure 2, let us consider a representative case in which $\gamma = 0.4$. For small values of B, the rotating stall point is found to be globally asymptotically stable for the system (8), (9). This is indicated by region (a) of Figure 2. However, for B greater than a critical value ($B = 0.367$ for $\gamma = 0.4$) the system (8), (9) has two periodic solutions (born at a cyclic fold bifurcation at $B = 0.367$) encircling the fixed point (i.e., the rotating stall point), with the stable periodic solution outside the unstable one as indicated at (b) of Figure 2. The rotating stall point, in this case, remains locally stable. As B increases, the unstable periodic solution shrinks and finally collapses onto the rotating stall point (which becomes unstable through an exchange

of stability), while the stable periodic solution grows and apparently reaches a limiting size, the so-called deep surge, as indicated at (c)-(e) of Figure 2.

The effects of throttle area (i.e., the value of γ) and the relaxation time constant τ on the axial flow compressor dynamics (1)-(4) are studied in more detail in the remainder of this section. In the following, we denote by B_c the critical value of B at which the two periodic solutions are born in a cyclic fold bifurcation. In Section 3.1, we discuss the effect of γ on the value of B_c for the reduced model (8), (9). The effects of γ and τ on the time response of the full model (1)-(4) are considered in Section 3.2.

3.1. Second-Order Simplified Model

First, we consider the effect of γ on the value of B_c for the second-order simplified model (8), (9). It is observed from Eqs. (8), (9) that the fixed points of the system depend on γ. Simulations demonstrate that the value of B_c increases with closing of the throttle (i.e., as γ is reduced) in Zone I. For the case in which $\gamma = 0.29$, we find $B_c = 0.74$, which is close to the value reported by Greitzer [1]. However, simulations show that Eqs. (8), (9) do not possess any periodic solutions for small γ. It is observed from simulation evidence that the smallest γ for which periodic solutions occur (indeed, two periodic solutions, through a cyclic fold bifurcation) is about 0.285. The rotating stall fixed point appears to be globally stable for $\gamma < 0.285$.

3.2. Fourth-Order Full Model

We now consider the behavior of the full fourth-order model, Eqs. (1)-(4), as a function of τ. The main finding is that the value of B_c depends on both γ and τ. As observed from simulations, for fixed γ, B_c grows with increasing time constant τ, while for fixed τ, B_c grows with decreasing γ. This observation agrees with the one given in Section 3.1. Referring to simulations, we have $B_c = 0.6835$ for ($\tau = 1.65$, $\gamma = 0.4$); $B_c = 0.6785$ for ($\tau = 1.2$, $\gamma = 0.36$); and $B_c = 0.673$ for ($\tau = 0.65$, $\gamma = 0.32$). These values are all close to the value 0.7 reported in [1]. However, they depend strongly on the throttle line setting and the relaxation time constant τ. In addition, it is observed that, under some conditions, system (1)-(4) does not possess periodic solutions. For instance, when $\tau = 0.1$, the system (1)-(4) has no periodic solutions for all $\gamma \leq 0.305$.

4. Normal (Unstalled) Zone Dynamics

In this and the next sections, we focus on the time response of the second order model (8), (9).

First, consider the case $\gamma > 0.442$ (i.e., Zone III dynamics). We have two typical responses for Eqs. (8), (9). One type of behavior is shown in the bifurcation diagram in Figure 3; this occurs for $0.442 < \gamma \leq 0.4617$. As B is increased, we witness the appearance of two large-amplitude periodic solutions via a cyclic fold bifurcation, followed by their later disappearance in a second cyclic fold bifurcation. The unstalled operating point is locally stable for all B. In the other (simpler) type of dynamic behavior, which occurs for $\gamma > 0.4617$, the unstalled equilibrium is globally asymptotically stable.

5. Pre-Stall Zone Dynamics

The dynamical behavior of the reduced model (7),(8) is found to be more complicated and to strongly depend on the setting of the throttle line in the pre-stall zone (Zone II), whose boundaries are defined by the saddle-node bifurcation of fixed points at $\gamma = 0.41$ and $\gamma = 0.442$. In order to compute a complete description of the different dynamical behaviors, the bifurcation analysis package AUTO [8] is used to compute fixed points, bifurcation points, periodic solutions, bifurcation points of periodic solutions, and their continuations. Phase portraits are constructed by computing saddle point stable (unstable) manifolds, which is achieved by integrating an initial condition near the saddle point along the stable (unstable) eigenvector backward (forward) in time—the simplicity of this scheme owes itself to the one-dimensional nature of the saddle manifolds. A shooting technique is used to compute the saddle connections and their continuations.

The classification of the dynamic behavior exhibited by the second order compressor model in the (γ, B)-plane is found in Figure 4. Each region (i.e., a to z) in Figure 4 denotes a qualitatively different behavior of the reduced model (8), (9) within a subset of (γ, B)-plane. Samples of these behaviors are depicted in Figure 5, which correspond to the behaviors in regions (a), (b), (n), (l), (k), (s), (x), (y) and (z), respectively. In these phase portraits, we may find one fixed point (for instance, a globally stable rotating stall equilibrium point as shown in Figure 5a) or three coexisting fixed points: the rotating stall

equilibrium point, the unstalled equilibrium point, and a saddle point (see, for instance, Figure 5b). The saddle point is marked with an "x" in the phase portraits.

The saddle point plays a crucial role in organizing the dynamics of Eqs. (8), (9) in the phase plane. For instance, following a perturbation in the unstable direction of the saddle point in Figure 5b will result in a trajectory (denoted by long-dashed curves) that asymptotically approaches one of the two stable fixed points (marked with filled-in circles) in forward time. These long-dashed curves form the unstable manifold of the saddle point. In addition, the stable manifold of the saddle point can also be constructed approximately by perturbing the saddle point along its stable direction and then following this point in backward time. This invariant curve (sometimes referred to as the separatrix), denoted by the solid line in Figure 5b, is defined by the set of all the initial conditions in phase space which asymptotically approach the saddle point in forward time. By this definition, we can see how the stable manifold acts as the boundary separating the domain of attraction of the unstalled operating point from that of the rotating stall point, which does provide a quantitative measurement of the robustness of the unstalled operating point under transient disturbances.

It is observed from Figure 4 that the variety of behaviors of Eqs. (8), (9) result from a combination of local bifurcations of the fixed points and global bifurcations. The local bifurcations include saddle-node bifurcations and Hopf bifurcations, while the global bifurcations consist of cyclic fold bifurcations (i.e., saddle-node bifurcations of periodic solutions) and homoclinic saddle connections.

The dynamical behaviors of Eqs. (8), (9) in both Zones I and II, in terms of the (γ, B)-plane, are illustrated in Figure 4. Next, we describe the dynamical behaviors indicated in Figure 4, with emphasis on Zone II behavior. For brevity, we only discuss some of results in detail. It is not difficult to recover the remaining behaviors of Eqs. (8), (9) from Figures 4 and 5.

First, we consider the separation between behavior (a) and behavior (b). These two behaviors are separated by a saddle-node bifurcation of fixed points, which gives birth to a saddle point and the stable unstalled operating point. (Note that such a bifurcation always gives rise to a stable operating point below the double-0 eigenvalue point [9] and

an unstable operating point above.) Next, we consider a bifurcation scenario consisting of a path through the (γ, B)-plane with a fixed value of γ ($\gamma = 0.424$) and B free. This one-parameter "slice" results in a bifurcation diagram passing from region (b) through regions (n), (l), (k), (s), (x), (y), and finally ends with behavior (z). The phase portrait of each region is shown in Figure 5, while the behaviors of (8), (9) at the separation of each two consecutive regions along the cut are described as follows.

Behavior (b) is separated from (n) by a cyclic fold bifurcation resulting in the birth of two periodic solutions which encircle all three fixed points, with the stable surge oscillation outside the unstable antisurge oscillation. The unstable periodic solution is observed to continuously shrink as B increases, and then its amplitude drops suddenly at the saddle-connection bifurcation which marks the separation of behaviors (n) and (l).

Another saddle-connection bifurcation separates behavior (l) from behavior (k) and gives rise to another, small-amplitude periodic solution encircling the unstalled equilibrium point as shown by behavior (k). In the phase portrait of (k), as depicted in Figure 5k, the two unstable periodic solutions define the basin of attraction of each stable fixed point. The unstable periodic solution encircling the rotating stall point shrinks as B increases and finally collapses onto the fixed point in the Hopf bifurcation separating behavior (k) from behavior (s). This process leaves the rotating stall point unstable, which is indicated by an open circle. The other unstable periodic solution grows with increasing B and is destroyed at a homoclinic saddle-connection bifurcation which separates behaviors (s) from (x). As B increases further, another saddle-connection bifurcation creates a large-amplitude unstable periodic solution (behavior (y)); this is depicted in Figure 5y. This periodic solution is almost immediately destroyed at a cyclic fold bifurcation which separates behavior (y) from (z). The dynamical behavior of (8), (9) is then observed to be qualitatively similar to behavior (z) as B is increased. The phase diagram of behavior (z) is depicted in Figure 5z.

Acknowledgment

The authors are grateful to Drs. W.M. Hosny, P.K. Houpt and L.P. Harris for helpful discussions. This work was supported in part by the General Electric Company, by NSF

Grant ECS-86-57561, by the NSF Engineering Research Centers Program: NSFD CDR-88-03012 and ECD-88-03012-06, and by the AFOSR University Research Initiative Program under Grant AFOSR-90-0015.

References

[1] E.M. Greitzer, "Surge and rotating stall in axial flow compressor, Part I: Theoretical compression system model," *ASME J. Engineering for Power*, 1976, pp. 190-198.

[2] E.M. Greitzer, "Surge and rotating stall in axial flow compressor, Part II: Experimental results and comparison with theory," *ASME J. Engineering for Power*, 1976, pp. 199-217.

[3] E.H. Abed, P.K. Houpt and W.M. Hosny, "Bifurcation analysis of surge and rotating stall in axial flow compressors," *Proc. 1990 American Control Conference*, San Diego, 1990, pp. 2239-2246.

[4] F.K. Moore and E.M. Greitzer, "A theory of post-stall transients in axial compression systems: Part I–Development of equations," *ASME J. Engineering for Gas Turbines and Power*, Vol. 108, 1986, pp. 68-76.

[5] E.M. Greitzer and F.K. Moore, "A theory of post-stall transients in axial compression systems: Part II–Application," *ASME J. Engineering for Gas Turbines and Power*, Vol. 108, 1986, pp. 231-239.

[6] F.E. McCaughan, "Application of bifurcation theory to axial flow compressor instability," *ASME J. Turbomachinery*, Vol. 111, 1989, pp. 426-433.

[7] F.E. McCaughan, "Numerical results for axial flow compressor instability," *ASME J. Turbomachinery*, Vol. 111, 1989, pp. 434-441.

[8] E.J. Doedel, "AUTO: A program for the automatic bifurcation analysis of autonomous systems," *Cong. Num.*, Vol. 30, 1981, pp. 265-284.

[9] J. Guckenheimer and P. Holmes, *Nonlinear Oscillations, Dynamical Systems, and Bifurcations of Vector Fields*, Appl. Math. Sciences Series, Vol. 42, Springer-Verlag, New York, 1983.

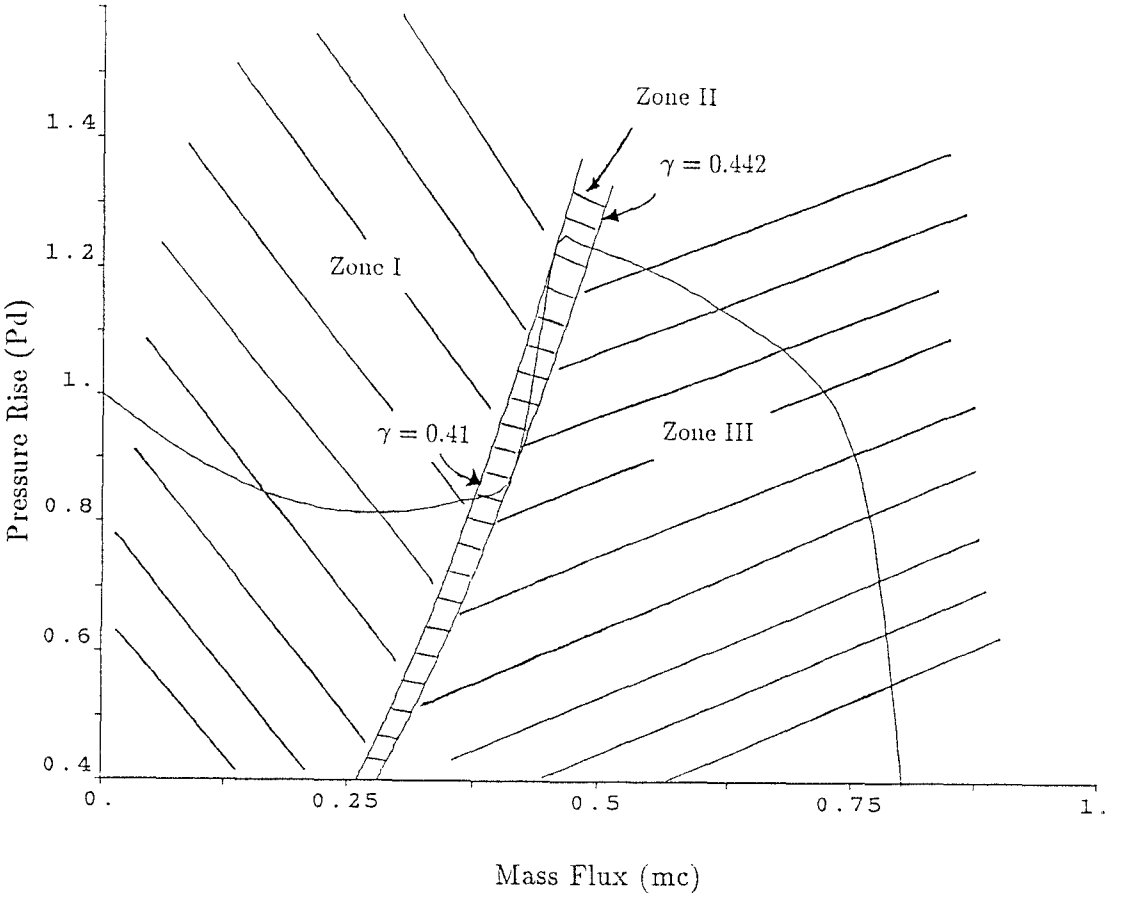

Figure 1. Characteristics of the axial flow compressor model in phase space.

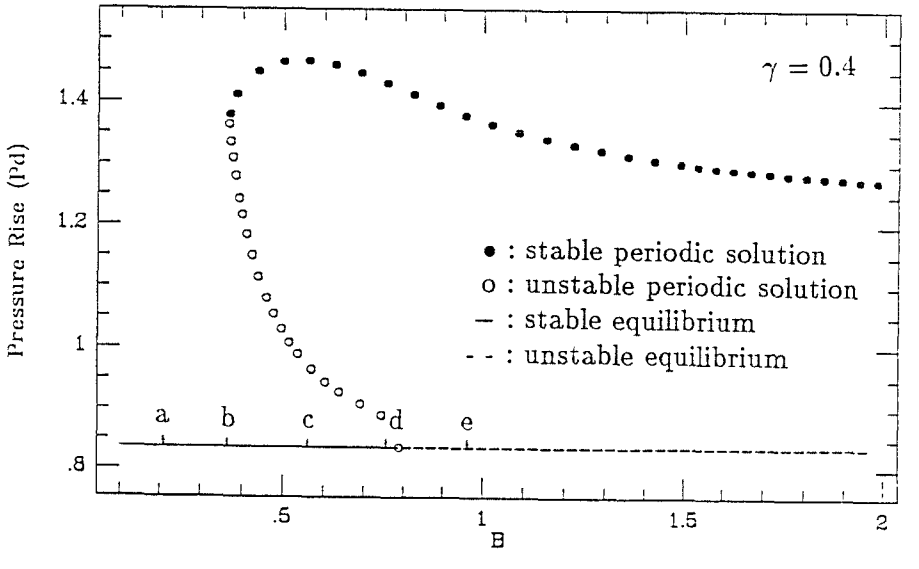

Figure 2. Bifurcation diagram for $\gamma = 0.42$.

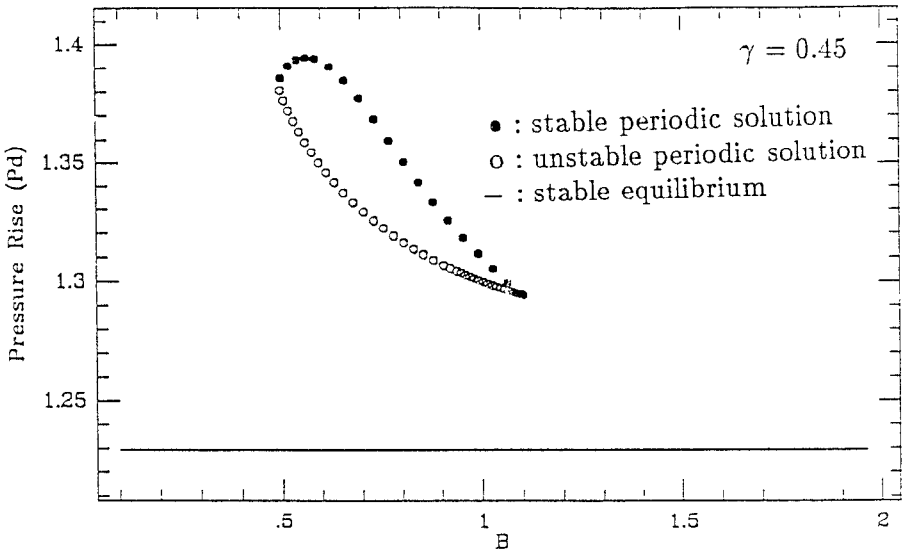

Figure 3. Bifurcation diagram for $\gamma = 0.45$.

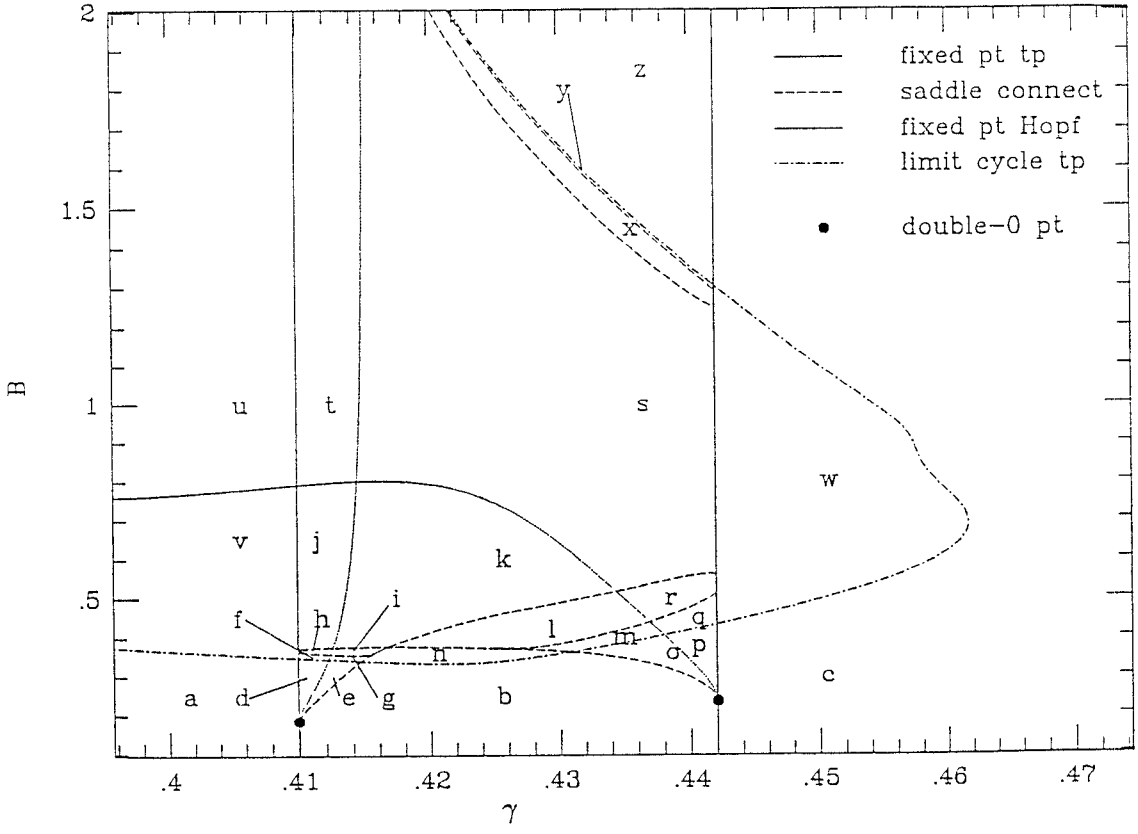

Figure 4. Classification of dynamical behavior of the compressor model in the (γ, B)-plane.

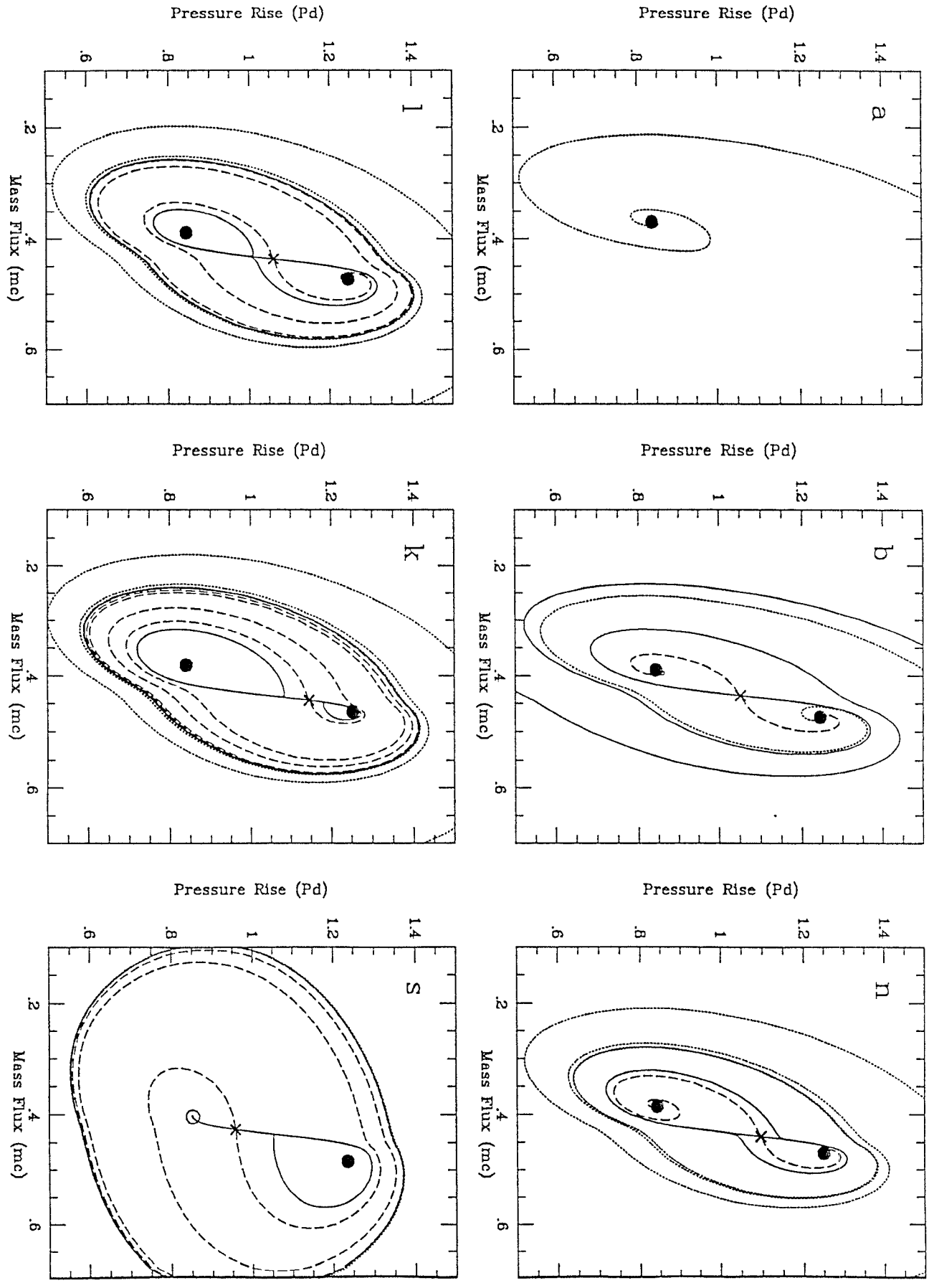

Figure 5. Phase portraits associated with behavior (a) and the one-parameter cut of $\gamma = 0.424$.

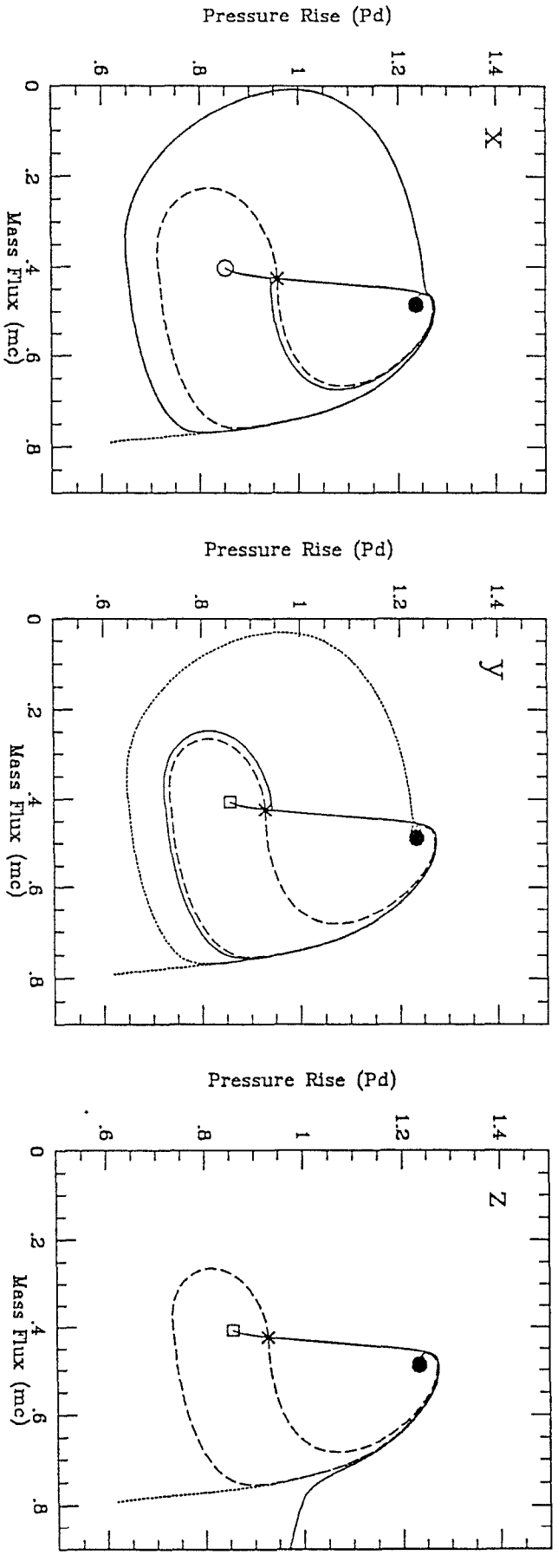

Figure 5. (continued) Phase portraits associated with behavior (a) and the one-parameter cut of $\gamma = 0.424$.